Wang *et al.*
Chinese Journal of Mechanical Engineering (2022) 35:104
https://doi.org/10.1186/s10033-022-00789-y

Chinese Journal of Mechanical Engineering

ORIGINAL ARTICLE

Open Access

Analysis of the Temperature Characteristics of High-speed Train Bearings Based on a Dynamics Model and Thermal Network Method

Baosen Wang[1,2,3], Yongqiang Liu[2*], Bin Zhang[3] and Wenqing Huai[4]

Abstract

High-speed trains often use temperature sensors to monitor the motion state of bearings. However, the temperature of bearings can be affected by factors such as weather and faults. Therefore, it is necessary to analyze in detail the relationship between the bearing temperature and influencing factors. In this study, a dynamics model of the axle box bearing of high-speed trains is established. The model can obtain the contact force between the rollers and raceway and its change law when the bearing contains outer-ring, inner-ring, and rolling-element faults. Based on the model, a thermal network method is introduced to study the temperature field distribution of the axle box bearings of high-speed trains. In this model, the heat generation, conduction, and dispersion of the isothermal nodes can be solved. The results show that the temperature of the contact point between the outer-ring raceway and rolling-elements is the highest. The relationships between the node temperature and the speed, fault type, and fault size are analyzed, finding that the higher the speed, the higher the node temperature. Under different fault types, the node temperature first increases and then decreases as the fault size increases. The effectiveness of the model is demonstrated using the actual temperature data of a high-speed train. This study proposes a thermal network model that can predict the temperature of each component of the bearings on a high-speed train under various speed and fault conditions.

Keywords: High-speed train, Axle box bearing, Temperature characteristics, Thermal network method

1 Introduction

As essential components of high-speed trains, axle box bearings play a critical role in their safe operation. Measuring temperature is currently the primary safety inspection method for high-speed train axle box bearings. Therefore, it is vital to analyze the factors influencing bearing temperature characteristics [1]. However, several factors affect the temperature of each component of the bearing, and the influencing mechanisms are complex. Furthermore, during the operation of trains, the external environment and operating conditions are constantly changing; therefore, the temperature is also constantly changing and is difficult to predict. In order to solve these problems, many experts and scholars have made significant efforts and research progress.

Choi [2] used a finite element model (FEM) to investigate the thermal characteristics of a spindle bearing system. Kucinschi et al. [3] proposed an advanced bi-dimensional model and used an FEM to calculate the temperature field in a journal bearing. As an FEM has good accuracy and can simulate the bearing temperature field well, it has also been applied to the analysis of high-speed trains. Tarawneh et al. [4] developed an FEM

*Correspondence: liuyq@stdu.edu.cn

[2] School of Mechanical Engineering, Shijiazhuang Tiedao University, Shijiazhuang 050043, China
Full list of author information is available at the end of the article

for railroad tapered roller bearings that could obtain the working temperature of the internal components of the bearing based on the external temperature. Yan et al. [5] established a heat generation model for both the raceway and rib of train bearings and employed the finite element method via the APDL (ANSYS parametric design language) program to analyze the temperature field distribution of the bearing under different speeds and loads. Although an FEM has high accuracy and can predict the overall temperature distribution of bearings, its calculation speed is slow. In practical applications, more attention is paid to the temperature of key components of bearings, which reduces the calculation efficiency of the FEM. The thermal network method can predict the temperature by closely linking the frictional heat, heat transfer relationship of each part of the bearing, and heat dissipation of the surrounding air. Power loss calculation is the most important step, and many scholars have studied the frictional heat of bearing systems.

Palmgren [6] fitted the empirical formula of the friction torque calculation through experimental research on bearings of different types and sizes. Nélias et al. [7] used angular contact ball bearings as the research object and proposed a calculation method for power loss. Harris et al. [8] used the friction torque formula to study the frictional heating power of the rolling-elements and raceways of ball bearings and roller bearings under oil lubrication conditions. Pouly et al. [9, 10] established a relatively complete thermal network model of angular contact ball bearings under oil and gas conditions. In the power loss, the frictional heat generated by the scroll and slide between the rollers and raceway, the viscous friction on the rollers, and the slide between the cage and ferrule were fully considered. However, the above energy loss models were considered in their entirety. During high-speed train operation, the contact force on each roller of the axle box bearing is constantly changing and needs to be calculated separately to achieve high fidelity [10]. Barday et al. [11] used the thermal network method to study the heat transfer of truck axles, in which the power loss of the gear set was determined by the local friction model. The calculation process for using the friction torque to obtain the power loss is complicated. If the model can directly calculate the contact force between the roller and raceway, more accurate results can be obtained with a greatly simplified solution process [12].

The thermal network model discretizes the bearing system into isothermal nodes based on its structure. There are different heat transfer relationships between these isothermal nodes, which can be divided into three types: heat conduction, convection, and radiation. As the heat transfer relationship between thermal network nodes is very complicated, a simplified model was used to calculate the thermal resistance between nodes. Eckert [13] studied the thermal convection relationship between the inner- and outer-rings of a bearing and lubricating oil. Ma et al. [14] studied the thermal convection relationship between a spindle and air using the theory of convective heat dissipation from a rotating cylinder. Jakob et al. [15] determined the surface heat transfer coefficient when forced heat convection occurred between the air outside the bearing housing and the outer surface of the bearing housing at a certain speed. In terms of heat conduction, the bearing seats, rings, and spindles are cylindrical or cylindrical entities along the radius. This type of one-dimensional heat conduction problem can be simplified to a single-layer cylindrical wall heat conduction problem [16]. Ai et al. [17] established a formula for the heat resistance between the rolling-elements and the raceway of the bearings. Muzychka et al. [18] studied the thermal resistance of an elliptical contact area and considered the influence of the contact area size and motion state on thermal resistance. In terms of air heat resistance, Meng et al. [19] provided a theoretical solution for the thermal resistance of a sealed air layer and used residential double-glazed glass as an example to determine its optimal thermal resistance value.

The thermal network method has been continuously studied, with an increasing number of applications since its inception. In 1974, Shaberth first developed a thermal calculation program for the US military that could calculate the temperature distribution and thermodynamic behavior of a spindle system containing up to five rolling bearings, which was updated and optimized in 1981 [20]. Dowson et al. [21] demonstrated a thermal network analysis method applied to a 110 mm diameter ring-oiled journal bearing.

Mezani et al. [22] presented a coupling model to describe the electromagnetic and thermal phenomena of an induction motor, in which the thermal analysis was conducted using the thermal network method. Although these studies explained the analysis process of the thermal network method in detail, it is equally important to study the influence of external conditions on the bearing temperature. Ai et al. [17] calculated the sliding friction loss and viscous drag loss of the rollers inner-ring, outer-ring, and large-end-flange in detail, and considered many factors that can affect the bearing temperature, such as contact force, grease, angular speed, and oil film thickness. Ma et al. [23] used the thermal network method to analyze temperature characteristics. The results indicated that the rotation speed, radial load, and grease filling rate were positively related to the bearing temperature. Zheng and Chen [24] developed a comprehensive thermal network model for a pair of front bearings of a

high-speed spindle and their surroundings to forecast the temperature rise of bearings and introduced the heat transfer path in the bearings in detail. In particular, the influence of the bearing thermal strain on the bearing force balance when calculating the heat generation was considered in the model. The experimental results indicated that the model was effective.

These studies used the thermal network method to simulate and analyze the bearing temperature. However, they are all based on static or pseudo-static models. During the operation of high-speed trains, the working conditions and temperature of the bearings constantly change. Furthermore, previous studies did not consider the impact of bearing faults and fault size on the temperature analysis, which is very important for high-speed trains. In addition, the atmospheric environment near the bearing was simplified. Owing to the high-speed of the trains, the air near the bearing is divided into two parts: near the spindle and near the axle box. Their temperatures are also different. To solve the above problems, this study proposes a dynamics and temperature coupling model for the axle box bearing of a high-speed train, in which the air near the axle box bearing is divided into two parts. Simultaneously, the model can describe the dynamics behavior and temperature changes of bearings with different fault sizes. A limitation of the model is that it is only applicable to the temperature at equilibrium points, that is, the model cannot describe the entire progress, which will be the focus of future work.

The remainder of this paper is organized as follows: Section 1 illustrates the research status of the two methods of temperature field analysis and the calculation steps of the thermal network method. Section 2 considers the high-speed train bearing dynamics model as the carrier, explains the calculation steps of the thermal network method in detail, and uses this method to obtain the temperature of each component of the bearing. Section 3 analyses the influence of bearing speed, fault type, and fault size on temperature, compares the real high-speed train axle temperature data and simulation results, and proves the validity of the model. Section 4 summarizes the work of the full text and points out the innovation of the article.

2 Thermal Network Method

2.1 Isothermal Nodes Division

The heat input in the temperature field needs to be solved by the dynamic model. The detailed modeling process of the dynamic model of the high-speed train bearing rotor system and the parameters of the system have been described in Refs. [25, 26], so this paper will not repeat the description in detail. The bearing system was assembled using different components [27]. It was assumed that in the heat transfer process, the temperatures at different positions in the same components were equal. Based on this, the bearing was divided into several isothermal nodes, as shown in Figure 1(a) and Table 1.

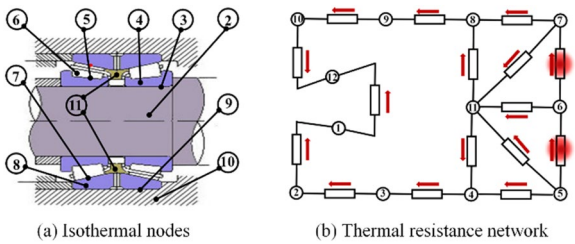

Figure 1 Bearing isothermal node division and heat transfer paths

Table 1 Isothermal nodes

Temperature of nodes	Name of nodes
T_1	Air around spindle
T_2	Spindle
T_3	Spindle ∩ inner ring
T_4	Inner ring
T_5	Inner ring ∩ rolling elements
T_6	Rolling elements
T_7	Outer ring ∩ rolling elements
T_8	Outer ring
T_9	Outer ring ∩ axle box
T_{10}	Axle box
T_{11}	Grease
T_{12}	Air around axle box

A ∩ B = Contact point of A and B

The contact point between the two contact objects of the bearing was also regarded as an isothermal node. According to the Hertz contact theory, the friction loss between the roller and raceway is generated in a small area, with a size much smaller than the diameter of the roller. This phenomenon limits the flow of heat from the contact area to the center of the contact body. That is, there is a 'bottleneck' in heat conduction between the surface of the bearing element and the main body [28]. According to Refs. [9, 10], the high-temperature zone of the bearing components is mainly concentrated on a very thin layer on the surface, whereas the temperature of the main body is relatively low. Furthermore, the bogie was constructed like a container with its opening facing down, through which the air around the spindle was enclosed and isolated from the air around the axle box. Therefore, the air around the spindle and the air around

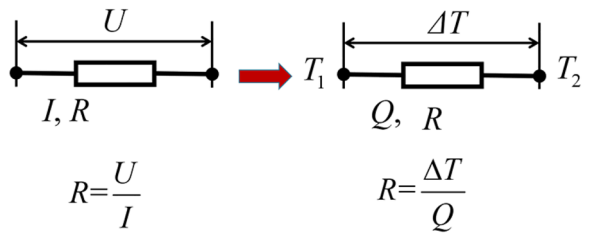

Figure 2 Popularization principle of thermal resistance

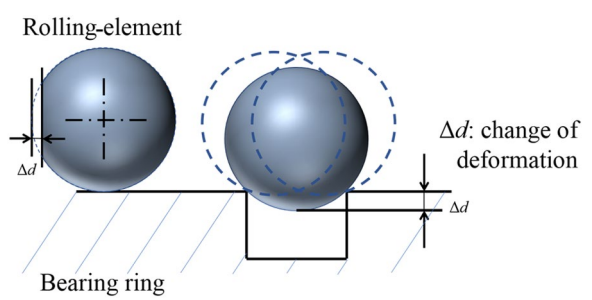

Figure 3 Change of deformation

the axle box were regarded as two different isothermal nodes.

In the system, heat was transferred between adjacent nodes that were connected by thermal resistance. In bearing operations, part of the heat generated inside the bearing is absorbed by the grease, and the other part is transmitted through various components of the bearing and finally dissipated into the air. The direction of heat flow is shown in Figure 1(b). The thermal resistance is defined by the generalized Ohm's law as:

$$R = \frac{\Delta T}{Q}, \tag{1}$$

where R is the thermal resistance, ΔT is the temperature difference, and Q is the heat flow between the two adjacent nodes. A generalized schematic of thermal resistance is shown in Figure 2.

2.2 Contact Force Analysis under Fault Conditions

The calculation of the contact force is the basis of model establishment and temperature field analysis. Existing studies [5, 29, 30] show that when a rolling-element passes through a fault area, the change in the deformation will cause sudden changes in the contact force, as shown in Figure 3. Simultaneously, an impact force was generated and modelled [31, 32]. When a fault exists in the bearing, the contact force will undergo a sudden change and an additional impact force will be generated to further increase the contact force. Based on the model established in this study, the resultant force of the contact force (referred to as the contact force hereafter) between the rolling-elements and the raceway was obtained when the bearing had outer-ring, inner-ring, and rolling-element faults, as shown in Figure 4. In this simulation, the fault size L_0 was 1 mm for an actual bearing wear width of approximately 1–3 mm, and the bearing inner-ring speed w_c was 1600 r/min, which was approximately 265 km/h, which is slightly lower than the current running speed of the high-speed train.

The characteristic fault frequencies of the bearing are denoted as f_{BPFO}, f_{BPFI}, and f_{BSF} for faults in the outer-ring, inner-ring, and rolling-element, respectively. Each time a rolling-element passed through the fault area, the contact force changed. The interval time of the contact force change t_{cit} is the same as the interval time for the rolling-element passing through the fault area. Furthermore, the rolling-elements contact the fault edge when entering and leaving the fault area, as shown in Figure 3, which causes two sudden changes in the contact force, and the time of the two sudden changes t_{sct} is proportional to the width of the fault. However, when a bearing has a rolling-element fault, the edge of the fault area is always in contact with the raceway. In this case, the deformation and contact force did not change. For the bearings used in the simulation, the following results were obtained.

When the bearing had an outer-ring fault:

$$\begin{cases} t_{cit} = \dfrac{1}{f_{\mathrm{BPFO}}} = 0.0053\ \mathrm{s}, \\ t_{sct} = \dfrac{N_0 \arcsin(\frac{L_0}{2r_0}) t_{cit}}{\pi} = 4.78 \times 10^{-4}\ \mathrm{s}. \end{cases} \tag{2}$$

When the bearing had an inner-ring fault:

$$\begin{cases} t_{cit} = \dfrac{1}{f_{\mathrm{BPFI}}} = 0.0037\ \mathrm{s}, \\ t_{sct} = \dfrac{N_0 \arcsin(\frac{L_0}{2r_0}) t_{cit}}{\pi} = 1.7 \times 10^{-4}\ \mathrm{s}. \end{cases} \tag{3}$$

When the bearing had a rolling-element fault:

$$\begin{cases} t_{cit} = \dfrac{1}{f_{\mathrm{BSF}}} = 0.013\ \mathrm{s}, \\ t_{sct} = \dfrac{N_0 \arcsin(\frac{L_0}{2r_0}) t_{cit}}{\pi} = 3 \times 10^{-4}\ \mathrm{s}. \end{cases} \tag{4}$$

A comparison of Eqs. (2)–(4) and Figure 4 show that the simulation and theoretical calculation results are consistent.

When the bearing speed was constant, the contact force P changed periodically within a certain period of time. Under the law of conservation of energy, it can be replaced by the average value of the contact force over a

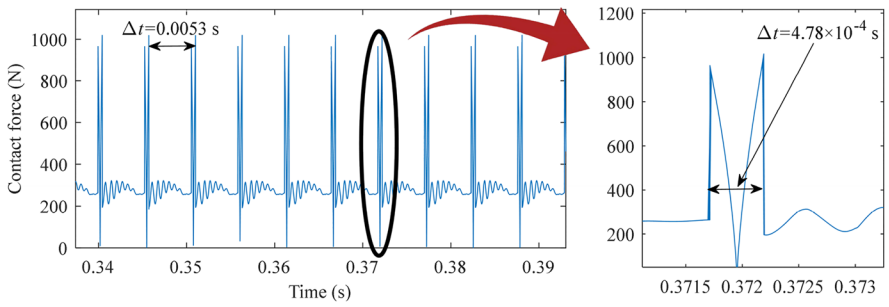

(a) Contact force under the condition of outer-ring fault

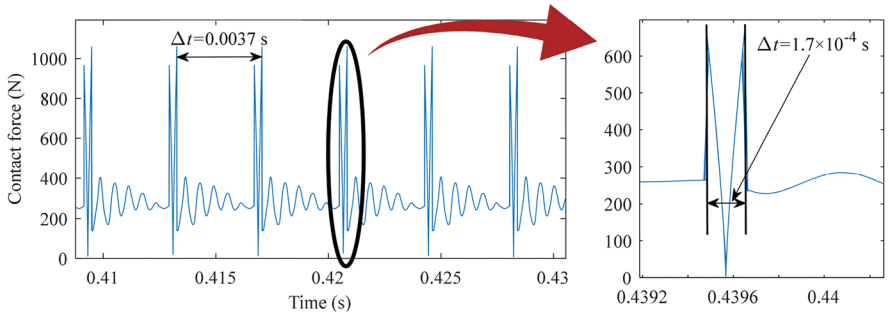

(b) Contact force under the condition of inner-ring fault

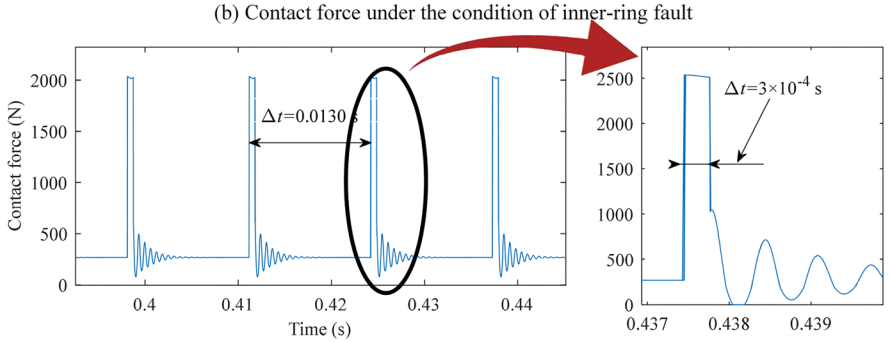

(c) Contact force under the condition of rolling-element fault

Figure 4 Resultant force of contact force between rolling-elements and raceway

given period. Figure 8 shows that the equivalent contact force changed when the fault size changed. As shown in Figure 5, when the bearing had no fault, the contact force was usually relatively small. In the presence of a fault, the contact force changed suddenly owing to the impact force. As the size of the fault increased, the contact force also increased. When the bearing had a rolling-element fault, the change in the contact force was more evident, and its characteristics were different from those of other fault scenarios. As the size of the rolling-element fault increased, the contact force dropped rapidly after a sudden change, and then gradually decreased. This is because the fault area became smoother as the width of the fault increased, making the impact force smaller, and thus the contact force smaller.

The internal power loss of rolling bearings was mainly caused by the mutual friction of the internal components of the bearing. This friction, including the friction between the rolling-elements and raceways of the inner- and outer-rings and the friction between the rolling-elements and the cage, is also the main reason for the increase in the bearing temperature. As the dynamics model in this study ignored abnormal bearing behaviors, such as roller slip and cage shaking, only the former friction was considered when calculating the energy loss, and the latter form of friction is equivalent to the contact force. In most cases, the friction torque is used to calculate the energy loss inside the bearing and obtain the total heat generation of the bearing. However, the positions of each roller of the bearing and the force are different. Local methods are more reasonable and easier to use

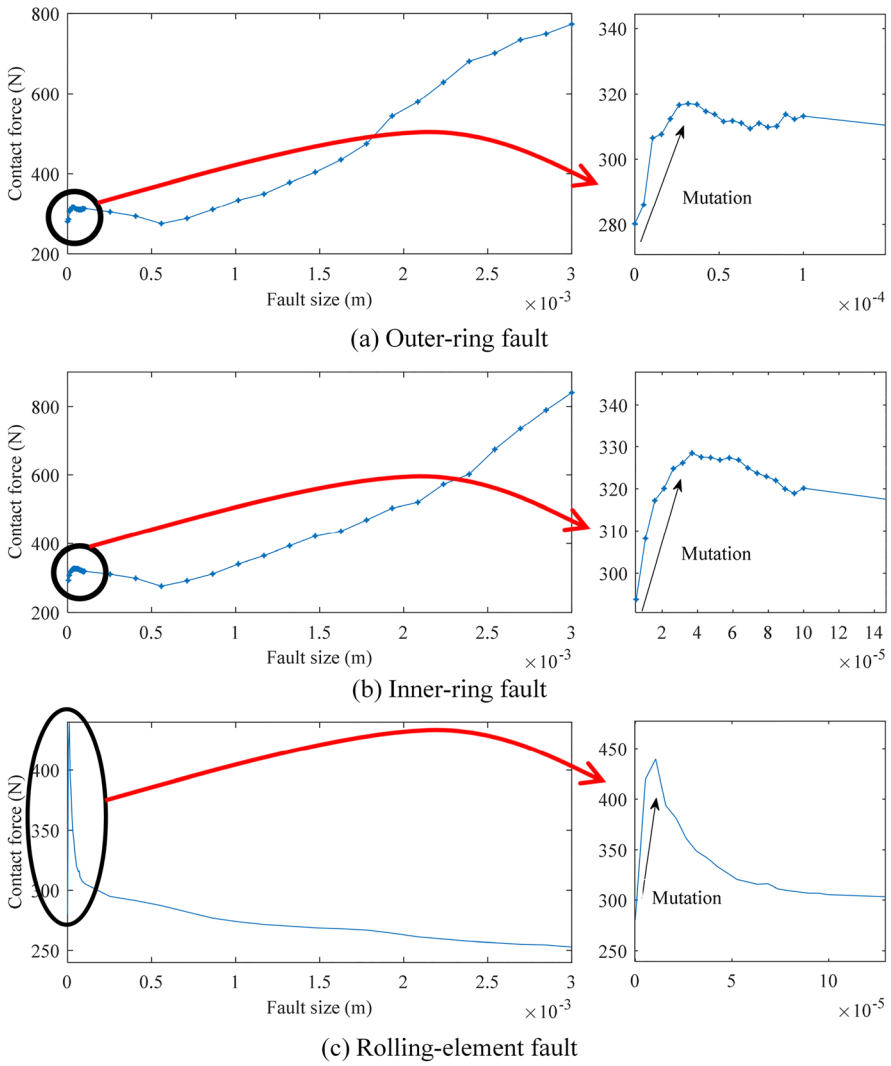

Figure 5 Relationship between contact force and fault size

[11]. In this method, the heat generation of each roller was calculated separately and then summed to obtain the overall heat generation of the bearing. The heat generation of each roller was calculated as follows:

$$q_i = \mu P_i v_i, \tag{5}$$

where q_i is the total frictional heat generation at the i-th roller, μ is the rolling friction coefficient between the roller and raceway, and v_i is the relative speed of the roller and raceway. The overall heat generation is given as:

$$Q = \sum_{i=1}^{N_0} q_i. \tag{6}$$

2.3 Thermal Resistance

Heat transfer in the bearing rotor system includes conduction heat transfer, convection heat transfer, and heat radiation. As the heat transfer by thermal radiation is much smaller than that of the other two modes, it can be ignored.

2.3.1 Conduction Heat Transfer

Heat conduction is a process in which a large number of molecules, atoms, or electrons collide with each other, and energy is transferred from a relatively high-temperature component or object to a low-temperature component or object.

(a) The bearing spindle, inner-ring, outer-ring, and axle box can be simplified as cylinders with inner- and outer-ring radii r_{in} and $r_{ex,}$ respectively. This type of heat conduction relationship can be simplified as a one-dimensional heat conduction problem along the radius [16], and the thermal resistance can be calculated as:

$$R = \frac{\ln r_{ex} - \ln r_{in}}{2\pi kL}, \tag{7}$$

where k is the thermal conductivity and L is the characteristic length. Thermal resistance between 'T_2&T_3', 'T_3&T_4', 'T_8&T_9', and 'T_9&T_{10}' in Figure 1 and Table 1, can be determined by Eq. (7).

(b) The contact between the roller and raceway is the Hertz contact, and the size of the contact area is much smaller than the size of the bearing. The thermal resistance of this component can be calculated as [18]:

$$R = \frac{1}{\pi}\left(\frac{a}{b}\right)\frac{1}{ka\sqrt{Pe}}, \tag{8}$$

where a is the semi-major axis of the ellipse along the rolling direction; b is the semi-minor axis of the ellipse perpendicular to the rolling direction; and Pe is the Peclet number. Eq. (8) is used to determine the thermal resistance between 'T_4&T_5', 'T_5&T_6', 'T_6&T_7', and 'T_7&T_8', as shown in Figure 1 and Table 1.

2.3.2 Convection Heat Transfer

Thermal convection is the heat exchange between a fluid and solid when the fluid flows over a solid surface. Heat convection is the most difficult form of heat transfer to quantify. In the bearing system, heat is transferred from the bearing to the lubricant, and then from the lubricant to the bearing seat and other components. Thermal convection also occurs between the outer surface of the bearing and the surrounding fluid, which is usually air. In most cases, the convection thermal resistance can be expressed as:

$$R = \frac{1}{Ah_c} = \frac{1}{A}\left(\frac{L}{kNu}\right), \tag{9}$$

where A is the surface area of the contact surface where heat exchange occurs, k is the thermal conductivity of the fluid, L is the characteristic length, and Nu is the dimensionless Nusselt number, which is determined by different convection conditions, as follows:

(a) The part of the spindle extending beyond the bearing exhibits a convective heat dissipation relationship with the air, and Nu is calculated as follows:

$$Nu = \begin{cases} 0.00308Re + 4.432 & Re < 7300, \\ Re^{0.37} & 7300 \le Re < 9600, \\ 30.5Re^{-0.0042} & Re \ge 9600, \end{cases} \tag{10}$$

where $Re = VD_s/\nu_{air}$, ν_{air} is the kinematic viscosity of air, V is the spindle line speed, and D_s is the spindle diameter. Eq. (10) is used to determine the thermal resistance between 'T_1&T_2' in Figure 1 and Table 1.

(b) When the bearing ring rotates, it exchanges heat with grease. The heat transfer relationship can be simplified as a concentric rotating cylinder model [33]. In this case, Nu was calculated as follows:

$$Nu = \begin{cases} 2 & Ta < 41, \\ 0.167Ta^{0.69}Pr^{0.4} & 41 \le Ta < 100, \\ 0.401Ta^{0.5}Pr^{0.4} & Ta \ge 100, \end{cases} \tag{11}$$

where $T_a = \rho\varepsilon_R\sqrt{\varepsilon_R r_{\text{ring}}}/\nu_g$ in which ε_R is the radial clearance between the inner- and outer-rings, r_{ring} is the internal radius of the ring, and ν_g is the kinematic viscosity of grease. Eq. (11) is used to determine the thermal resistance between 'T_4&T_{11}', 'T_5&T_{11}', 'T_6&T_{11}', 'T_7&T_{11}', and 'T_8&T_{11}', in Figure 1 and Table 1.

(c) When the train is moving, air blows over the surface of the axle box at the speed of the train, which causes forced convection to dissipate heat. The surface heat transfer coefficient h_c can be approximated as

$$h_c = 0.03\frac{k}{D_h}(u_s D_h/\nu_{\text{air}})^{0.57}, \tag{12}$$

where k is the air thermal conductivity, and D_h is the outer diameter of the axle box.

As air is a fluid, there is natural convection heat dissipation between the air and axle box. In this case, Nu can be determined using Eq. (10). Assuming that the equivalent thermal resistance of the air and axle box is R, the resistance of forced convection heat dissipation is R_1, and the resistance of natural convection heat dissipation is R_2. Then, we have

$$\frac{1}{R} = \frac{1}{R_1} + \frac{1}{R_2}. \tag{13}$$

Eq. (13) can be used to determine the thermal resistance between 'T_{10}&T_{12}' in Figure 1 and Table 1.

2.3.3 Heat Transfer in the Enclosed Air Layer

Under normal circumstances, high-speed trains travel very quickly, which reduces the efficiency of the heat exchange between the air near the spindle of the bogie and the outside atmosphere. The air near the spindle is confined in a closed space and isolated from the outside atmosphere by an air layer. The air near the spindle dissipates the heat absorbed from the spindle to the outside atmosphere through the air layer. The thermal resistance between 'T_1&T_{12}' in Figure 1 and Table 1 can be calculated by:

$$R = \frac{d_{\text{air}}}{\lambda_a + \lambda_c + \lambda_r}, \tag{14}$$

where d_{air} is the thickness of the enclosed air layer, λ_{a} is the thermal conductivity of the air layer, λ_{c} is the convective equivalent thermal conductivity of the air layer, and λ_{r} is the radiation equivalent thermal conductivity of the air layer.

2.4 Node Temperature Solution

In electricity, the nodal current law states that the sum of the currents flowing into a node is equal to the sum of the currents flowing out of the node. Similarly, in a thermal grid, the sum of the heat flowing into a node is equal to the sum of the heat flowing out of the node. An equivalent schematic is shown in Figure 6. In particular, additional heat is generated near the rolling-elements owing to friction, and the heat relationship at the relevant nodes is:

$$\sum Q_{\text{in}} + \sum Q_f - \sum Q_{\text{out}} = 0, \tag{15}$$

where Q_{in} is the input heat, Q_{out} is the output heat, and Q_{f} is the heat generated by friction.

According to Ohm's law, Eq. (15) can be used to determine the heat flow relationship at each node in the thermal network and finally obtain a set of equations representing the direction of heat flow in the bearing rotor system. The thermal resistance between the two nodes is distinguished by the node number, where c is the heat transfer by conduction, and v is the heat transfer by convection. For example, R_{3c2} represents the conduction thermal resistance between T_3 and T_2 and the heat flows from T_3 to T_2. Similarly, R_{6v11} represents the convection thermal resistance between T_6 and T_{11} and the heat flows from T_6 to T_{11}. The thermal resistance of the enclosed air layer is R_{air}. Based on the analysis above, the heat transfer in the bearing system can be described as follows:

$$\begin{cases}
\frac{T_1 - T_{12}}{R_{\text{air}}} - \frac{T_2 - T_1}{R_{2v1}} = 0, \\
\frac{T_2 - T_1}{R_{2v1}} - \frac{T_3 - T_1}{R_{3c2}} = 0, \\
\frac{T_3 - T_1}{R_{3c2}} - \frac{T_4 - T_3}{R_{4c3}} = 0, \\
\frac{T_4 - T_3}{R_{4c3}} - \frac{T_{11} - T_4}{R_{11v4}} - \frac{T_5 - T_4}{R_{5c4}} = 0, \\
\frac{T_5 - T_4}{R_{5c4}} + \frac{T_5 - T_{11}}{R_{5v11}} + \frac{T_5 - T_6}{R_{5c6}} = 1/(2Q_{\text{i}}), \\
\frac{T_6 - T_{11}}{R_{6v11}} - \frac{T_5 - T_6}{R_{5c6}} - \frac{T_7 - T_6}{R_{7c6}} = 1/(2Q_{\text{i}}) + 1/(2Q_{\text{o}}), \\
\frac{T_7 - T_8}{R_{7c8}} + \frac{T_7 - T_{11}}{R_{7v11}} + \frac{T_7 - T_6}{R_{7c6}} = 1/(2Q_{\text{o}}), \\
\frac{T_8 - T_9}{R_{8c9}} - \frac{T_{11} - T_8}{R_{11v8}} - \frac{T_7 - T_8}{R_{7c8}} = 0, \\
\frac{T_9 - T_{10}}{R_{9c10}} - \frac{T_8 - T_9}{R_{8c9}} = 0, \\
\frac{T_{10} - T_{12}}{R_{10v12}} - \frac{T_9 - T_{10}}{R_{9c10}} = 0, \\
\frac{T_{11} - T_4}{R_{11v4}} + \frac{T_{11} - T_8}{R_{11v8}} - \frac{T_7 - T_{11}}{R_{7c11}} - \frac{T_6 - T_{11}}{R_{6v11}} - \frac{T_5 - T_{11}}{R_{5v11}} = 0,
\end{cases} \tag{16}$$

where Q_{i} and Q_{o} are the heat generated by the friction between the rolling-elements and raceway of the inner- and outer-rings, respectively. The temperature of the outside atmosphere, T_{12}, was constant in this study. In Eq. (16), there were 11 equations and 11 unknowns. The temperature of each node can be obtained using the Gauss-Seidel iteration method [34].

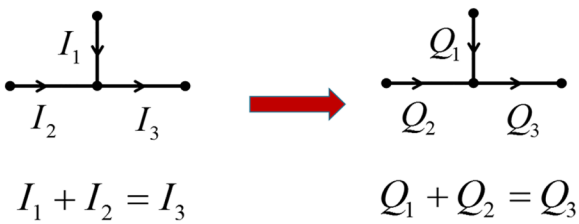

Figure 6 Derivation of heat relationship principle

3 Results and Discussion

3.1 Effect of Speed on Temperature

When a train is running, the speed often changes, which also causes a change in the temperature of various components of the bearing. To describe this phenomenon, the bearing dynamics model and thermal grid model were used to obtain the temperature of each node of the bearing and its change with speed. To illustrate the influence of the bearing speed temperature, the temperature at each node under the condition of no fault and a bearing angular speed of 1600 r/min was obtained by simulation, as shown in Table. 2. Node T_{12}, the temperature of the air around the axle box, is given as T_{12} = 20 °C.

It can be seen from Table 2 that the temperatures of nodes T_5–T_7 were relatively higher. This is because the heat generated by the internal friction of the bearing radiated from the vicinity of the rolling-elements. Simultaneously, because grease (T_{11}) absorbed part of the heat

Table 2 Isothermal nodes

Node number	Node temperature (℃)	Node number	Node temperature (℃)
T_1	32.43	T_7	92.86
T_2	81.07	T_8	69.13
T_3	81.64	T_9	58.53
T_4	81.97	T_{10}	53.24
T_5	88.81	T_{11}	79.81
T_6	86.96	T_{12}	20

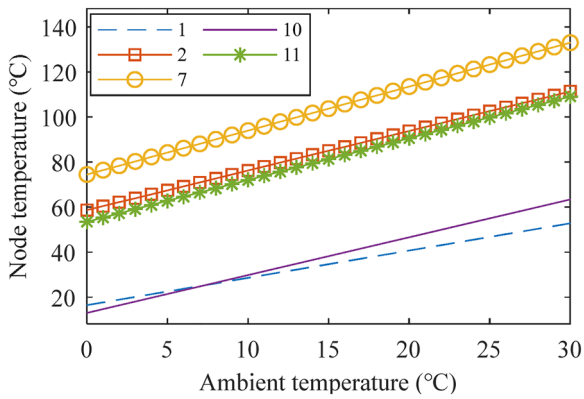

Figure 7 Node temperature change with the temperature of the air around axle box

generated by friction, its temperature was also very high. Among them, the temperature of node T_7 was the highest because the outer-ring bears a large load from the car body. The temperature of the air around the axle box (T_{12}) is an important part of the thermal grid that directly or indirectly affects the temperature of the components of the bearing rotor system. Ref. [35] lists the actual measured temperature data of high-speed train, in which the bearing temperature of the trailer reached 69.8 °C, which is very close to the calculated result of 69.13 °C (T_8). The actual measured temperature of the trailer axle box (50 °C–65 °C) is also consistent with the calculated results (T_{10}). Figure 7 shows the temperature change of representative nodes with the temperature of the air around the axle box.

As shown in Figure 7, the outside air temperature, that is, the temperature of the air around the axle box, had a linear relationship with the temperature of the system components. This eliminated the interference of the outside atmospheric temperature when analyzing the influence of other factors on the temperature of each component. Figure 8 shows the temperature changes of representative nodes with the train running speed. In the simulation, the inner-ring speed was 400–2000 r/min and the step was 200 r/min, corresponding to a train running speed of 66–332 km/h.

As shown in Figure 8, as the train speed increased, the convection heat dissipation between the box body and the surrounding air accelerated. Consequently, the heat generated by the internal friction of the bearing was quickly transferred to the external environment, causing the internal temperature of the bearing to decrease gradually. However, when the train speed was greater than approximately 133 km/h, the heat generated by friction could not be dissipated easily into the air through air convection, thereby increasing the internal temperature of the bearing. Therefore, when the train speed was higher than 133 km/h, the higher the train speed, the higher the temperature of each bearing component. The difference is that the temperature of the axle box (T_{10}) continued to decrease as the speed of the train increased. This is because the relative speed between the train and the outside air increased, so that the heat in the box was dissipated into the air faster through convection. Furthermore, the lower the speed, the higher the temperature of the grease, and the higher the speed, the higher the temperature of the spindle. This means that as the train speed increased, more heat inside the bearing was transferred to the air through various components, and the heat

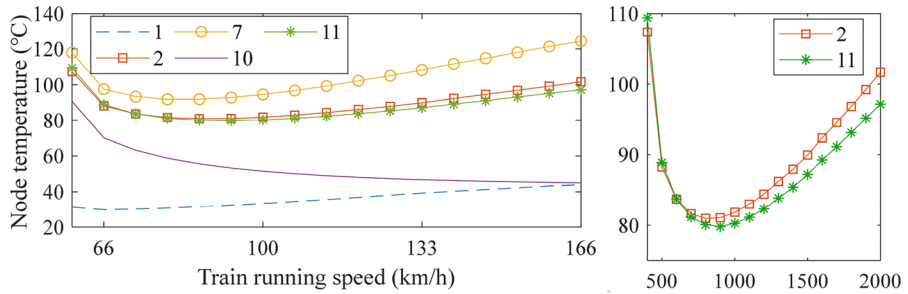

Figure 8 Node temperature change with the train running speed

absorbed by the grease decreased. This was evidenced by the increasing temperature of the air near the spindle.

3.2 Effect of Faults on Temperature

In addition to speed, the type of bearing fault and size of the fault also significantly affect the temperature. Based on the temperature of T_7, a comparative analysis under different types of faults and different speed conditions was performed, as shown in Figure 9(a), and a comparative analysis under the conditions of different fault sizes and a bearing angular speed of 1600 r/min was performed, as shown in Figure 9(b), in which ORF = outer-ring fault, IRF = inner-ring fault, and REF = rolling-element fault.

As shown in Figure 9(a), compared with the outer- and inner-ring faults, the temperature of T_7 was more sensitive to rolling-element faults. Once the rolling-element failed, the temperature increased sharply. As the size of the fault increased, the faulted edge became smoother. Therefore, the contact force and temperature gradually decreased. When the bearing fault had a small size (approximately less than 0.6 mm) on the outer- and inner-rings, the temperature change was almost the same. When the fault size was large, the temperature increased with an increase in fault size. Moreover, under the inner-ring fault condition, the temperature increased faster. As shown in Figure 9(b), as the bearing speed increased, the temperature under the three fault conditions first decreased and then increased. The temperature was the highest under the rolling-element fault condition. Under the conditions of the outer- and inner-ring faults, the temperature was almost the same. The results demonstrate that temperature is very sensitive to speed and is more sensitive to rolling-element faults.

3.3 Verification of Actual Train Axle Temperature

To verify the thermal coupling bearing dynamics model established in this study, real temperature data of a certain type of high-speed (Electrical Multiple Units) EMU and the simulation results were used for a comparative analysis. The data included the temperature of the bearing outer-ring and spindle. The data were obtained on the China Rejuvenation train on February 5, 2020. The maximum running speed of the train was 350 km/h. A diagram of the installation of the sensors is shown in Figure 10. The sensor used for the axle temperature data was fixed to the vehicle and the sensor model was PT100. The acquisition instrument and the temperature display are shown in Figure 11.

During the operation of the train, the data acquisition instrument sampled the temperature and speed once every 30 s, that is, with a sampling frequency of 1/30 Hz. During data pre-processing, some invalid data and abnormal values were deleted. As a result, the time axis was not continuous, and the number of data points was different. For example, there were 33 data points in Figure 12(b) and 240 data points in Figure 13(b). In the simulation, the bearing had no faults, and the bearing rotating speed was the train's running speed. In addition, when the train speed is 0, in a real environment, the temperature of each component of the bearing gradually drops to the outside temperature. In the simulation model, when there was no heat input, the temperature of each component of the bearing was eventually equal to the outside temperature. Therefore, in the simulation, when the train was stationary, the temperature of each component of the bearing was regarded as the outside temperature. A comparative analysis of the bearing outer-ring (T_8) temperature is shown in Figure 12, and a comparative analysis of the spindle (T_2) temperature is shown in Figure 13.

Figures 12 and 13 show a comparison of the actual temperature data and the simulation results. When the speed of the train increased, both the actual collected temperature and simulated temperature increased rapidly. When the speed of the train decreased, both gradually

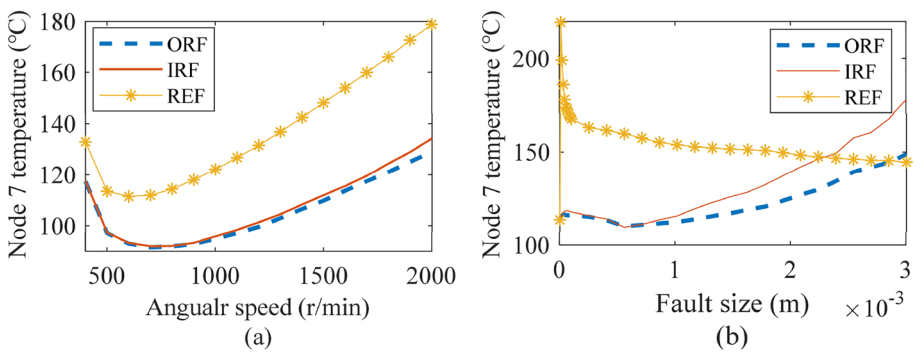

Figure 9 Change of temperature with different conditions

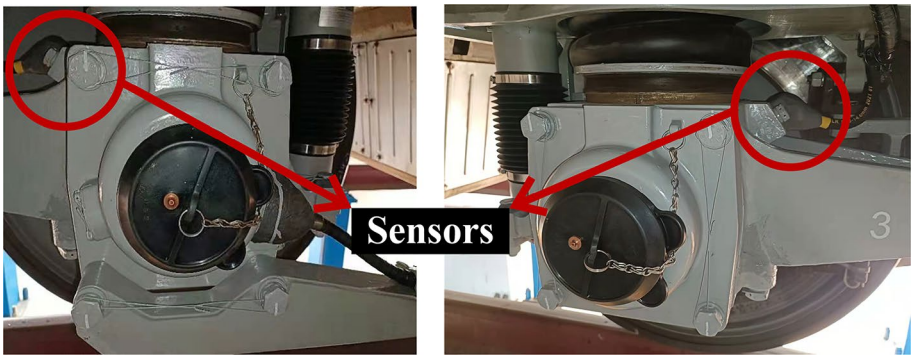

Figure 10 Bogie and the installation diagram of sensor

Figure 11 Acquisition instrument and temperature display

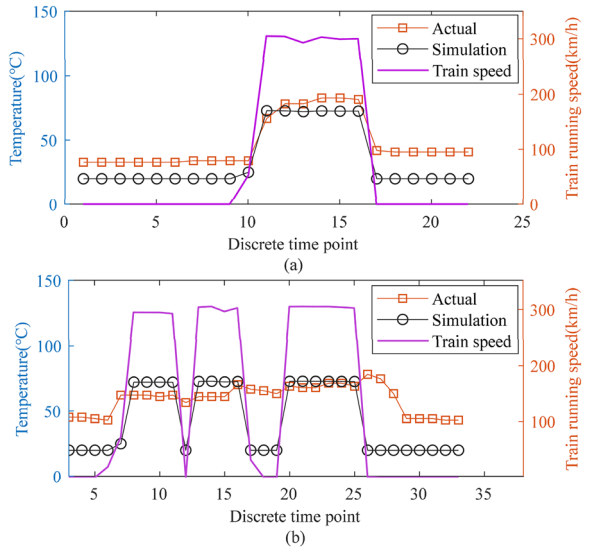

Figure 12 Comparative analysis of outer-ring temperature

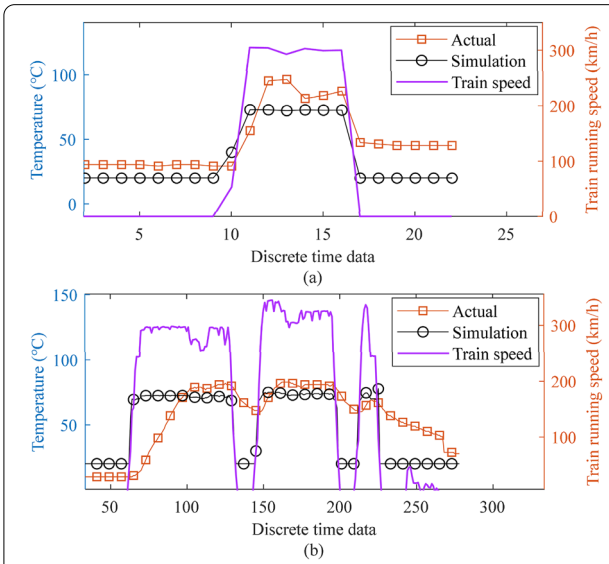

Figure 13 Comparative analysis of spindle temperature

decreased. When the train speed was 0, the actual train bearing temperature slowly dropped to the ambient temperature. During this period, the actual temperature was higher than the simulation result. This is because the model only simulated the final state of the bearing temperature.

In Figures 12(a) and 13(a), because the heat production and heat dissipation in the bearing system had not yet reached the equilibrium state during the continuous operation of the train, the temperature continued to rise during this period. As shown in Figures 12(b) and 13(b), when the train was stationary, the temperature of the outer bearing ring gradually decreased. Then, before the temperature reached the outside temperature, the train restarted, and the temperature increased. As the model only simulated the final state of the temperature, it cannot fully describe the temperature change process. This will be an avenue for future work.

4 Conclusions

(1) Based on a dynamic model of the bearing rotor systems of high-speed trains established in the previous work, the contact force changes were analyzed when the bearing had outer-ring, inner-ring, and rolling-element faults. The simulation results of the model were consistent with the theoretical calculation results.

(2) A thermal grid model of a high-speed train bearing rotor system was established, and the power loss was obtained using the local method. The simulation results of the model show that the temperature of the contact point between the outer-ring and the rolling-elements was the highest, and the relationship between the temperature of the contact point and the type of fault, size of the fault, and speed of the bearing spindle were further analyzed.

(3) Under no-failure conditions, the bearing temperature data collected by real high-speed EMUs and the simulation results were used for a comparative analysis. These results prove the validity of the model. However, the developed model could only simulate the final temperature when the bearing temperature reached an equilibrium state. Future work will focus on developing a model that can describe the dynamics temperature process.

Acknowledgments
The authors sincerely thank to Xiaohui Gu, Jingyu Hou and Jing Zhao for their work on the fault-bearing experiment of a high-speed train.

Author Contributions
YL was in charge of the whole trial; BW and BZ wrote the manuscript; WH reviewed the manuscript and provided the data. All authors read and approved the final manuscript.

Authors' Information
Baosen Wang, born in 1990, is currently a PhD candidate at *School of Traffic and Transportation, Shijiazhuang Tiedao University, China*. He received his master's degree from *Shijiazhuang Tiedao University, China*, in 2018. His research interests include dynamics modeling analysis and bearing fault diagnosis of high-speed train bearings.

Yongqiang Liu, born in 1983, is currently a professor at *School of Mechanical Engineering, Shijiazhuang Tiedao University, China*. He received his PhD degree in vehicle engineering from *Beijing Jiaotong University, China*, in 2011. His research interests include prognostics and health management, vehicle system dynamics, and smart soft material and damper.

Bin Zhang, born in 1972, is currently an associate professor at *Department of Electrical Engineering, University of South Carolina, USA*. He received his PhD degree in electrical engineering from *Nanyang Technological University, Singapore*, in 2007. His research interests include prognostics and health management, intelligent systems and controls, and their applications to various engineering systems.

Wenqing Huai, born in 1993, is currently an assistant engineer at *Taiyuan Vehicle depot of Daqin Railway Co., Ltd., China*. He received his master's degree from *Shijiazhuang Tiedao University, China*, in 2018. His research interests include temperature characteristic analysis of bearing rotor system and health status management of power supply under train.

Funding
Supported by National Key R&D Program (Grant No. 2020YFB2007700), National Natural Science Foundation of China (Grant Nos. 11790282, 12032017, 12002221 and 11872256), S&T Program of Hebei (Grant No. 20310803D), and Natural Science Foundation of Hebei Province (Grant No. A2020210028), and State Foundation for Studying Abroad.

Competing interests
The authors declare no competing financial interests.

Author Details
[1]School of Traffic and Transportation, Shijiazhuang Tiedao University, Shijiazhuang 050043, China. [2]School of Mechanical Engineering, Shijiazhuang Tiedao University, Shijiazhuang 050043, China. [3]Department of Electrical Engineering, University of South Carolina, Columbia 29201, USA. [4]Taiyuan Vehicle Depot of Daqin Railway Co., Ltd., Taiyuan 030000, China.

Received: 11 September 2021 Revised: 22 June 2022 Accepted: 22 July 2022
Published online: 11 August 2022

References

[1] A L Wang, J G Wang. Temperature distribution and scuffing of tapered roller bearing. *Chinese Journal of Mechanical Engineering*, 2014, 27(6): 1272-1279.
[2] J K Choi. Thermal characteristics of the spindle bearing system with a gear located on the bearing span. *International Journal of Machine Tools and Manufacture*, 1998, 38(9): 1017-1030.
[3] B R Kucinschi, M Fillon, J Fréne, et al. A transient thermoelastohydrodynamics study of steadily loaded plain journal bearings using finite element method analysis. *Journal of Tribology*, 2000, 122(1): 219-226.
[4] C M Tarawneh, A A Fuentes, J A Kypuros, et al. Thermal modeling of a railroad tapered roller bearing using finite element analysis. *Journal of Thermal Science and Engineering Applications*, 2012, 4(3): 031002.
[5] K Yan, N Wang, Q Zhai, et al. Theoretical and experimental investigation on the thermal characteristics of double-row tapered roller bearings of high-speed locomotive. *International Journal of Heat and Mass Transfer*, 2015, 84: 1119-1130.
[6] A Palmgren. *Ball and roller bearing engineering*. Philadelphia: SKF Industries Inc, 1959.
[7] D Nelias, P Sainsot, L Flamand. Power loss of gearbox ball bearing under axial and radial loads©. *Tribology transactions*, 1994, 37(1): 83-90.
[8] T Harris, M Kotzalas, N Michael. *Rolling bearing analysis: advanced concepts of bearing technology*. Boca Raton: CRC Press, 2007.
[9] F Pouly, C Changenet, F Ville, et al. Investigations on the power losses and thermal behavior of rolling element bearings. *Proceedings of the Institution of Mechanical Engineers, Part J: Journal of Engineering Tribology*, 2010, 224(9): 925-933.
[10] F Pouly, C Changenet, F Ville, et al. Power loss predictions in high-speed rolling element bearings using thermal networks. *Tribology Transactions*, 2010, 53(6): 957-967.

[11] D Barday, C Fossier, C Changenet, et al. Investigations on drive axle thermal behaviour: power loss and heat-transfer estimations. *SAE International Journal of Engines*, 2018, 11(1): 55-66.
[12] W C Tang, M J Wang, G D Chen. Analysis on temperature distribution of failure axle box bearings of high-speed train. *Journal of the China Railway Society*, 2016, 38(7): 50-56.
[13] Eckert E R G. *Introduction to the transfer of heat and mass*. New York: McGraw-Hill, 1950.
[14] H T Ma, W Y Zhou, X Y Lu, et al. Investigation on the air flow and heat transfer from a horizontal rotating cylinder. *International Journal of Thermal Sciences*, 2015, 95: 21-28.
[15] M Jakob, G A Hawkins, et al. *Elements of heat transfer and insulation*, 2nd ed. New York: John Wiley & Sons, Inc, 1950.
[16] J P Holman. *Heat transfer (Si Units) Sie*. 10th ed. Tata McGraw-Hill Education Pvt. Ltd, 2011.
[17] S Y Ai, W Z Wang, Y L Wang, et al. Temperature rise of double-row tapered roller bearings analyzed with the thermal network method. *Tribology International*, 2015, 87: 11-22.
[18] Y S Muzychka, M M Yovanovich. Thermal resistance models for non-circular moving heat sources on a half space. *Journal of Heat Transfer*, 2001, 123(4): 624-632.
[19] Q L Meng, N Cai, Q G Chen. A theoretical solution on the thermal resistance of sealed air layer. *Journal of South China University of Technology: Natural Science Edition*, 1997, 4: 116-119.
[20] G B Hadden, R J Kleckner, M A Ragen, et al. Steady state and transient thermal analysis of a shaft bearing system including ball, cylindrical and tapered roller bearing. *NASA technical paper*, 1981: 254.
[21] D Dowson, A O Mian, C M Taylor. Paper XIX (i) Thermal network analysis of a ring-oiled bearing and comparison with experimental results. *Tribology Series*, 1987, 11: 579-586.
[22] S Mezani, N Takorabet, B Laporte. A combined electromagnetic and thermal analysis of induction motors. *IEEE transactions on Magnetics*, 2005, 41(5): 1572-1575.
[23] F B Ma, Z M Li, S C Qiu, et al. Transient thermal analysis of grease lubricated spherical roller bearings. *Tribology International*, 2016, 93: 115-123.
[24] D X Zheng, W F Chen. Effect of structure and assembly constraints on temperature of high-speed angular contact ball bearings with thermal network method. *Mechanical Systems and Signal Processing*, 2020, 145: 106929.
[25] Y Q Liu, B S Wang, B Zhang, S P Yang. Establishment of dynamic model for axle box bearing of high-speed trains under variable speed conditions. *Chinese Journal of Mechanical Engineering*, 2022: 35, 47. https://doi.org/10.1186/s10033-022-00725-0
[26] Y Q Liu, B S Wang, S P Yang. Nonlinear dynamics behaviors analysis of bearings rotor system with outer ring faults in the high-speed train. *Journal of Mechanical Engineering*, 2018, 54(8): 17-25.
[27] S H Zhou, G Q Song, Z H Ren, et al. Nonlinear dynamic analysis of coupled gear-rotor-bearing system with the effect of internal and external excitations. *Chinese Journal of Mechanical Engineering*, 2016, 29(2): 281-292.
[28] T A Harris, M N Kotzalas. *Advanced concepts of bearing technology: rolling bearing analysis*. 5th ed. Boca Raton: CRC Press, 2006.
[29] S A McInerny, Y Dai. Basic vibration signal processing for bearing fault detection. *IEEE Transactions on education*, 2003, 46(1): 149-156.
[30] A Rafsanjani, S Abbasion, A Farshidianfar, et al. Nonlinear dynamics modeling of surface defects in rolling element bearing systems. *Journal of Sound and Vibration*, 2009, 319(3-5): 1150-1174.
[31] S Khanam, J K Dutt, T N andon. Impact force-based model for bearing local fault identification. *Journal of Vibration and Acoustics*, 2015, 137(5): 051002.
[32] M J Zhang, J Tang, X M Zhang, et al. Intelligent diagnosis of short hydraulic signal based on improved EEMD and SVM with few low-dimensional training samples. *Chinese Journal of Mechanical Engineering*, 2016, 29(2): 396-405.
[33] I S Bjorklund, W M Kays. Heat transfer between concentric rotating cylinders. *Journal of Heat Transfer*, 1959, 81(3): 175-183.
[34] Y M Xu, M M Ai, Y Yang. Heat transfer characteristic research based on thermal network method in submersible motor. *International Transactions on Electrical Energy Systems*, 2018, 28(3): e2507.
[35] Z W Wang, Y Cheng, P Allen, et al. Analysis of vibration and temperature on the axle box bearing of a high-speed train. *Vehicle System Dynamics*, 2020, 10(58): 1605-1628.